JACS JOURNAL OF THE AMERICAN CHEMICAL SOCIETY

Communication

Cite This: J. Am. Chem. Soc. 2018, 140, 15564−15567

pubs.acs.org/JACS

Exceptional Adsorption and Binding of Sulfur Dioxide in a Robust Zirconium-Based Metal−Organic Framework

Joseph H. Carter,[†,‡] Xue Han,[†] Florian Y. Moreau,[†] Ivan da Silva,[§] Adam Nevin,[†] Harry G. W. Godfrey,[†] Chiu C. Tang,[‡] Sihai Yang,*[,†] and Martin Schröder*[,†]

[†]School of Chemistry, University of Manchester, Manchester M13 9PL, United Kingdom

[‡]Diamond Light Source, Harwell Science Campus, Oxfordshire OX11 0DE, United Kingdom

[§]ISIS Facility, STFC Rutherford Appleton Laboratory, Oxfordshire OX11 0QX, United Kingdom

Supporting Information

ABSTRACT: We report a record-high SO_2 adsorption capacity of 12.3 mmol g^{-1} in a robust porous material, MFM-601, at 298 K and 1.0 bar. SO_2 adsorption in MFM-601 is fully reversible and highly selective over CO_2 and N_2. The binding domains for adsorbed SO_2 and CO_2 molecules in MFM-601 have been determined by *in situ* synchrotron X-ray diffraction experiments, giving insights at the molecular level to the basis of the observed high selectivity.

The International Energy Outlook 2017 report produced by the U.S. Energy Information Administration predicts that fossil fuels will account for ∼77% of global energy production in 2050, with coal comprising a major component of the overall energy supply.[1] The burning of bituminous, subbituminous and lignite coals produces SO_2 at a concentration of between 500 and 3000 ppm, around 95% of which is removed via limestone-scrubbing or the wet-sulfuric-acid processes.[2] Although these processes are effective, as much as 400 ppm of SO_2 can remain in the exhaust gas, which, when vented to the atmosphere, poses significant health risks and environmental impact.[3] Small amounts of SO_2 in flue gas can also react with organo-amines used for CO_2-scrubbing causing permanent loss of activity.[4] Physisorption of SO_2 by porous materials such as zeolites,[5] mesoporous silica,[6] ionic microgels[7] and activated carbons[8] using supramolecular host−guest interactions is a promising approach that can give high selectivity, reversibility and low energy penalty for system regeneration. However, these materials generally suffer from low adsorption capacities and exposure to SO_2 often leads to irreversible structural degradation.

Metal−organic frameworks (MOFs) are emerging porous materials constructed from metal clusters with organic linkers,[9] and their tuneability makes them interesting candidates for many applications.[10] Although much work has focused on the study of gas separations in MOFs, very little effort has been devoted to the sequestration of SO_2,[11] since it often leads to severe structural degradation of the material and/or irreversible uptake. Here, we report the exceptional adsorption and reversible binding of SO_2 in two Zr-based MOFs, MFM-600 and MFM-601. MFM-601 is obtained by postsynthetic removal of a linker in an ordered, predictable pattern from MFM-600. This is accompanied by significant enhancement of gas adsorption in MFM-601, notably simultaneous increases in SO_2 uptake (146%) and selectivity over CO_2 and N_2. Significantly, MFM-601 shows a SO_2 adsorption capacity of 12.3 mmol g^{-1} at 298 K and 1.0 bar, representing the highest value observed to date in porous materials under the same conditions. In addition, the binding domains for adsorbed CO_2 and SO_2 in MFM-610 have been determined by *in situ* synchrotron X-ray diffraction.

4,4′,4″,4‴-(1,4-Phenylenebis(pyridine-4,2,6-triyl))tetra benzoic acid (H_4L, Scheme 1) was prepared via a three-step synthesis (Scheme S1). $[Zn_6(\mu_3\text{-}O)_4(\mu_3\text{-}OH)_4(OH)_4(L)_2(H_4L)_{0.7}]$ (MFM-600) was synthesized by heating a mixture of $ZrCl_4$, H_4L and benzoic acid as modulator in DMF at 120 °C for 24 h and was isolated as plate-shaped colorless single crystals. The single crystal X-ray structure shows that MFM-600 contains $[Zr_6(\mu_3\text{-}O)_4(\mu_3\text{-}OH)_4(OH)_4]^{8+}$ clusters, first observed in UiO-66.[12] In this cluster the six Zr^{IV} ions form an octahedron with the 8 faces each capped by a μ_3-O or μ_3-OH. Eight of the edges of the octahedron are bridged by L^{4-} linkers via bidentate carboxylate groups with the remaining four equatorial edges each bridged by a H_4L linker (occ = 0.35) that is monodentate to each equatorial Zr(IV) center and bound through the C═O moiety of the carboxylate groups (Figure S4). The coordination sphere at the equatorial Zr(IV) centers is completed by a terminal OH^- ligand.

Scheme 1. Synthesis of MFM-601 from 4,4′,4″,4‴-(1,4-Phenylenebis(pyridine-4,2,6-triyl))tetrabenzoic Acid (H_4L)

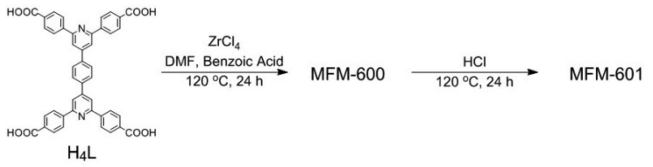

MFM-600 was treated with an 8 M solution of HCl, which led to a structural phase transition to MFM-601, $[Zn_6(\mu_3\text{-}O)_4(\mu_3\text{-}OH)_4(OH)_4(H_2O)_4(L)_2]$, the structure of which was determined by high resolution synchrotron powder X-ray diffraction with the $\{Zr_6\}$ node assigned to the MIX-staggered

Received: August 7, 2018
Published: November 12, 2018

DOI: 10.1021/jacs.8b08433
J. Am. Chem. Soc. 2018, 140, 15564−15567

proton topology.[13] In MFM-601, the H_4L monodentate linkers from the equatorial positions of the $\{Zr_6\}$ cluster have been removed (Figure 1) and replaced with terminal H_2O

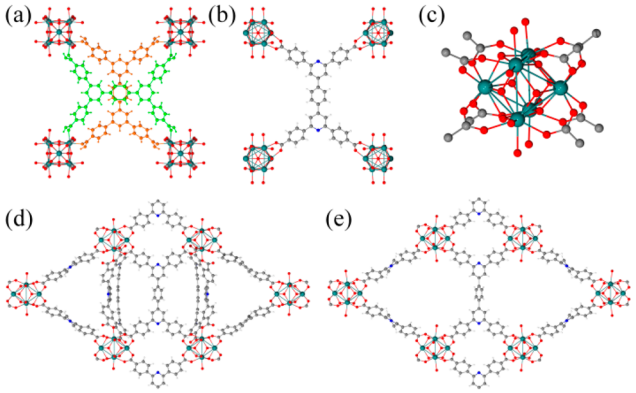

Figure 1. Views of (a) disordered H_4L linker present in MFM-600; (b) "fully bound" L^{4-} linker present in MFM-600 and MFM-601; (c) $\{Zr_6\}$ node present in MFM-600 and MFM-601; (d) structure of MFM-600; (e) structure of MFM-601.

molecules. As a result, the alternating linkage between the $[Zr_6(\mu_3\text{-}O)_4(\mu_3\text{-}OH)_4(OH)_4(H_2O)_4]^{8+}$ cluster and the L^{4-} linker yields two types of channels of ~9 Å (cylinder-shaped) and ~12 Å (waterdrop-shaped) diameter running through the structure of MFM-601 along the *c*-axis. This leads to an increase in the BET surface area from 2281 m^2g^{-1} for MFM-600 to 3644 m^2g^{-1} for MFM-601, a rise of ~60%. We note that MFM-601 has recently been reported (as BUT-15) as an adsorbent for Fe^{III} ions in water.[14] Acid treatment has been previously reported as an efficient approach to remove free ligands such as surplus benzoic acid modulator in Zr-based MOFs[15] and as a method of improving the N_2 uptake in UiO-66.[16]

Sorption isotherms of SO_2, CO_2 and N_2 were measured on desolvated samples. As expected, the higher BET surface area of MFM-601 allows a greater total uptake of all three gases. MFM-600 displays a two-step Type-IV isotherm for SO_2 with an excess uptake of 5.0 mmol g^{-1} at 298 K and 1.0 bar. Interestingly, in comparison, MFM-601 exhibits a type-I isotherm for SO_2 leading to an exceptionally high uptake of 12.3 mmol g^{-1} (146% enhancement) at 298 K and 1.0 bar, representing the highest value observed in porous solids and notably higher than a range of best-behaving SO_2 sorbents (Table S1). Importantly, no loss of adsorption capacity of SO_2 was observed in MFM-601 over five cycles of adsorption/desorption (Figure S17b). The SO_2 uptake in MFM-601 is further increased to 16.9 mmol g^{-1} at 273 K and 1.0 bar (Figure S17a). MFM-601 shows fully reversible adsorption of SO_2 at both 273 and 298 K, allowing the total evacuation of the framework upon desorption under pressure-swing conditions (Figure 2) with no structural phase change or framework collapse, as evidenced by the postsorption PXRD patterns (Figure S8). This is in contrast to the current leading SO_2 sorbent, MFM-202a, which undergoes irreversible phase change to MFM-202b upon SO_2 adsorption,[17] and Ni(bdc)-$(ted)_{0.5}$ and MOF-74(Mg), which release up to 40% of the captured SO_2 upon desorption.[18] The desorption of SO_2 from SIFSIX-1-Cu has not been reported.[20a] Interestingly, the high uptake of SO_2 in MFM-601 does not correlate with equivalent increases in uptake of CO_2 or N_2. The uptake of CO_2 in MFM-

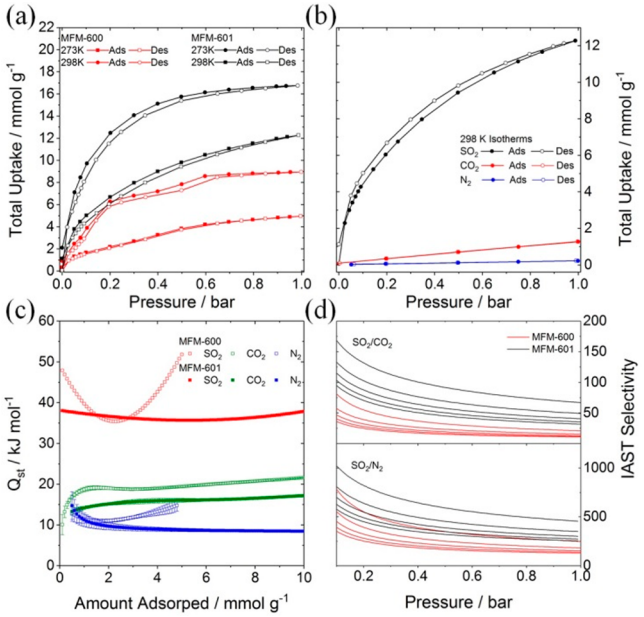

Figure 2. (a) SO_2 sorption isotherms in MFM-600 and MFM-601. (b) Comparison of SO_2, CO_2 and N_2 isotherms at 298 K in MFM-601. (c) Q_{st} values for SO_2, CO_2 and N_2 in MFM-600 and MFM-601. (d) IAST selectivities of SO_2/CO_2 and SO_2/N_2 at 298 K in MFM-600 and MFM-601 as a function of substrate ratios.

601 exhibits a type V isotherm with slow initial uptake at low pressures before the uptake increases more rapidly at intermediate pressures reaching a plateau at ~24 mmol g^{-1} at 30 bar and 298 K (Figure S15). Adsorption of N_2 in MFM-601 follows a type-I isotherm with a total uptake of ~12 mmol g^{-1} at 80 bar 298 K. Strikingly, despite the high uptake of SO_2 at 298 K and 1.0 bar, under the same conditions the CO_2 uptake in MFM-601 compares poorly to other MOFs in the literature,[19] with a total CO_2 uptake of only 1.3 mmol g^{-1} and a negligible N_2 uptake. The isosteric heat of adsorption (Q_{st}) for SO_2, CO_2 and N_2 in MFM-600 and MFM-601 are compared in Figure 2c. The same trend is followed for both MOFs with N_2 having the lowest Q_{st}, followed by CO_2 and then SO_2 with the highest Q_{st}. Interestingly the Q_{st} values for SO_2 in MFM-600 are generally higher than in MFM-601, consistent with the smaller cages of MFM-600 affording greater overlap potentials between SO_2 molecules and the pore interior. In MFM-600 at low loadings SO_2 interacts with binding sites at the MOF surface. As these sites become less available Q_{st} reduces, but once SO_2 fills the pore, SO_2–SO_2 dipole interactions lead to an increase in Q_{st}.

Analysis of adsorption selectivities at 298 K using ideal adsorbed solution theory (IAST) shows that the transformation of MFM-600 to MFM-601 is accompanied by an increase in selectivity of SO_2 over both CO_2 and N_2 (Figure 2). The selectivity for equimolar mixtures of SO_2/CO_2 and SO_2/N_2 in MFM-601 at 298 K are 32 and 255, respectively, comparable with the leading MOFs in the literature.[20] The capability of selective separation of SO_2 from gas mixtures using fixed-bed packed with MFM-601 has been confirmed by dynamic breakthrough experiments (Figure 3 and SI).

In order to examine the origins of the preferential adsorption of SO_2 over CO_2 in MFM-601, *in situ* synchrotron X-ray powder diffraction studies were carried out (Figures 4 and 5). Rietveld refinement of PXRD data for CO_2-loaded MFM-601

DOI: 10.1021/jacs.8b08433
J. Am. Chem. Soc. 2018, 140, 15564–15567

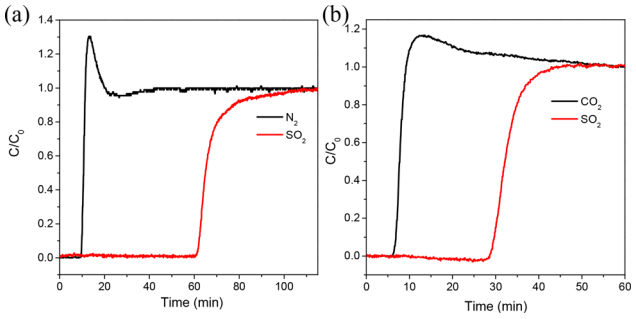

Figure 3. Breakthrough curves of 2500 ppm of SO_2 diluted in (a) 1:1 He:N_2 and (b) 1:1 He:CO_2 through a fixed-bed packed with MFM-601 at 298 K and 1 bar.

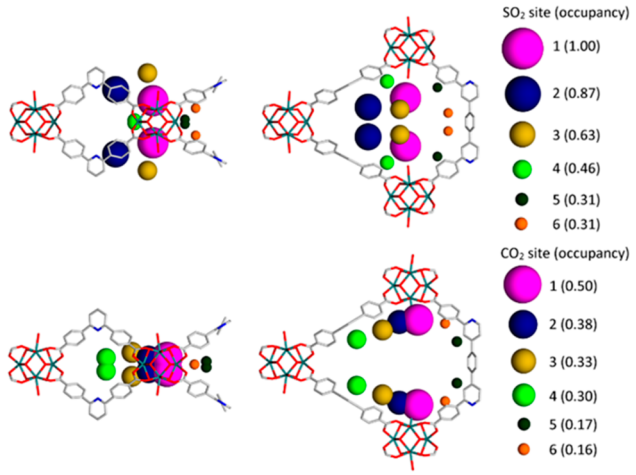

Figure 4. View of SO_2 (top) and CO_2 (bottom) in MFM-601; the size of the colored balls represent the occupancy at each site. Positions refined by *in situ* synchrotron PXRD.

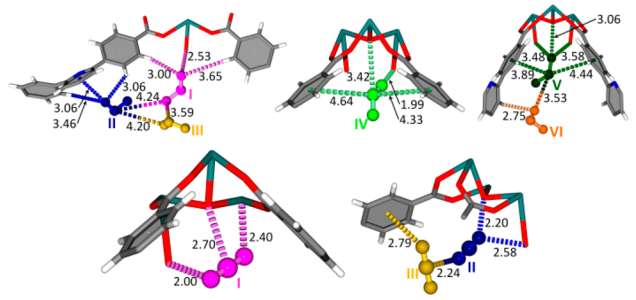

Figure 5. Binding sites of SO_2 (top) and CO_2 (bottom) in MFM-601.

at 200 K revealed six binding sites within the pores, giving a formula of $[Zr_6(\mu_3\text{-}O)_4(\mu_3\text{-}OH)_4(OH)_4(L)_2][CO_2]_{5.52}$. The primary binding site of CO_2^{I} in MFM-601 (occupancy = 0.50) overlaps with the terminal oxygen of the zirconium cluster due to the removal of four H_2O molecules from each $\{Zr_6\}$ cluster upon activation, leaving a terminal hydroxyl and an open zirconium site on each of the four equatorial edges of the $[Zr_6(\mu_3\text{-}O)_4(\mu_3\text{-}OH)_4(OH)_4]^{8+}$ cluster, thus accounting for the 0.5 occupancy of the terminal oxygen and CO_2^{I}. This positioning of CO_2^{I} puts it within close proximity to the open zirconium site $[O_{CO2}\cdots Zr = 2.40(10)$ Å] as well as being within binding distance of the terminal hydroxyl $[C_{CO2}\cdots O = 2.00(24)$ Å] and the μ_3-O of the Zr_6O_8 cluster $[C_{CO2}\cdots\mu_3\text{-}O = 2.70(11)$ Å], similar to that observed in UiO-66.[21] CO_2^{II} (occupancy = 0.38) and CO_2^{VI} (occupancy = 0.16) occupy similar environments either side of the zirconium cluster in that they are both in close proximity to the terminal hydroxyl $[(O_{CO2}\cdots O = 2.58(23)$ Å) and $[O_{CO2}\cdots O = 3.31(44)$ Å], respectively, as well as the μ_3-O $[(O_{CO2}\cdots\mu_3\text{-}O = 2.20(10)$ Å) and $[O_{CO2}\cdots\mu_3\text{-}O = 3.37(14)$ Å], respectively. The remaining sites, CO_2^{III} (occupancy = 0.33), CO_2^{IV} (occupancy = 0.30) and CO_2^{V} (occupancy = 0.17), are not within binding distance of the $\{Zr_6\}$ cluster but are closer to the L^{4-} linker. CO_2^{III} is near the phenyl ring of the linker $[O_{CO2}\cdots Ph = 2.79(8)$ Å] whereas CO_2^{IV} and CO_2^{V} are close to the pyridyl rings $[O_{CO2}\cdots N_{Pyr} = 4.38(5)$ Å)] and $[O_{CO2}\cdots H_{Pyr} = 3.91(25)$ Å], respectively. All CO_2 sites are within intermolecular binding distance of one another with C···O distances between 2.18(14) and 4.38(12) Å. However, no ordered CO_2 molecule was present at the center of the large pore of MFM-601, thus confirming that CO_2 positioning is dominated by host–guest interactions.

The crystal structure of SO_2-loaded MFM-601 at 298 K also shows six binding sites within the pore giving a formula of $[Zr_6(\mu_3\text{-}O)_4(\mu_3\text{-}OH)_4(OH)_4(H_2O)_4(L)_2][SO_2]_{10.71}$. The three SO_2 positions with the highest occupancies, SO_2^{I} (occupancy = 1.00), SO_2^{II} (occupancy = 0.87) and SO_2^{III} (occupancy = 0.63) form an intermolecular dipole bonding network with S···O bond distances between 3.59(7) and 3.24(6) Å, thus exhibiting efficient packing as exhibited by the similarity to the intermolecular distances observed in solid SO_2.[22] The highest occupied SO_2 position (SO_2^{I}) is located near the terminal hydroxyl of the $\{Zr_6\}$ cluster $[O_{SO2}\cdots O = 2.53(6)$ Å] with a similar SO_2-hydroxyl interaction to that observed in MFM-300(In).[20b] SO_2^{II} sits away from the zirconium cluster, close to the pyridyl group of the L^{4-} linker $[O_{SO2}\cdots Pyr = 3.06(6)$ Å].

Conversely, SO_2^{III} is not in close proximity to the pore wall and is only within interaction distance of other SO_2 molecules. SO_2^{IV} (occupancy = 0.46) occupies a position between two phenyl rings of two opposite linkers related by a mirror plane. It is in close proximity to both the terminal hydroxyl $[O_{SO2}\cdots O = 1.99(10)$ Å] and the μ_3-O $[S_{SO2}\cdots\mu_3\text{-}O = 3.42(5)$ Å] of the $[Zr_6(\mu_3\text{-}O)_4(\mu_3\text{-}OH)_4(OH)_4(H_2O)_4]^{8+}$ cluster. As for SO_2^{IV}, SO_2^{V} (occupancy = 0.31) resides in between the phenyl rings of two opposite L^{4-} linkers and also is in close proximity to the terminal hydroxyl $[O_{SO2}\cdots O = 3.48(15)$ Å] and the μ_3-O $[O_{SO2}\cdots\mu_3\text{-}O = 3.06(15)$ Å] of the $\{Zr_6\}$ cluster. The least occupied SO_2 site (SO_2^{VI}; occupancy = 0.31) lies near to a pyridyl ring of the organic linker $[O_{SO2}\cdots H_{Pyr} = 2.75(19)$Å] and also exhibits the potential for dipole–dipole interaction with SO_2^{V} $[O^{VI}\cdots S^{V} = 3.53(18)$Å] (Figures 4 and 5).

In conclusion, exceptional adsorption of SO_2 and selective sorption of SO_2 over CO_2 and N_2 have been demonstrated in a robust Zr-based MOF, MFM-601. By locating the positions of CO_2 and SO_2 in MFM-601, key understanding of the observed uptake and selectivity has been gained. It has been shown that the dipole moment of SO_2 can be utilized by MFM-601 not only to provide stable binding within the pores but also to drive intermolecular interactions between SO_2 molecules.

■ ASSOCIATED CONTENT

Supporting Information

The Supporting Information is available free of charge on the ACS Publications website at DOI: 10.1021/jacs.8b08433.

Data for $(C_{475.2}H_{248}N_{21.6}O_{139.2}Zr_{24})$ (CIF)
Data for $C_{44}H_{24}N_2O_{16}Zr_3$ (CIF)
Data for $C_{44}H_{24}N_2O_{14}Zr_3$, $7.36(CO_2)$ (CIF)

DOI: 10.1021/jacs.8b08433
J. Am. Chem. Soc. 2018, 140, 15564–15567

Data for $C_{44}H_{24}N_2O_{16}Zr_3$, $14.272(SO_2)$ (CIF)

Synthesis, characterization, and analysis of crystal structures (PDF)

AUTHOR INFORMATION

Corresponding Authors

*Sihai.Yang@manchester.ac.uk;

*M.Schroder@manchester.ac.uk

ORCID

Sihai Yang: 0000-0002-1111-9272

Martin Schröder: 0000-0001-6992-0700

Notes

The authors declare no competing financial interest.

CCDC-1850112, 1854228, 1854229 and 1854234 contain the supplementary crystallographic data.

ACKNOWLEDGMENTS

We thank EPSRC (EP/I011870), ERC (AdG 742041) and University of Manchester for funding. We thank Diamond Light Source for access to Beamline I11 and for awarding J.H.C. a Ph.D. scholarship.

REFERENCES

(1) U.S. Energy Information Administration. *International Energy Outlook 2017*; U.S. Energy Information Administration: Washington, DC, 2017.

(2) Gary, J. H.; Handwerk, G. E. *Petroleum Refining Technology and Economics*, 4th ed.; Marcel Dekker: New York, 2001.

(3) (a) Committee on Acute Exposure Guideline Levels, Committee on Toxicology, *Board on Environmental Studies and Toxicology. Acute Exposure Guideline Levels for Selected Airborne Chemicals*; National Academies Press: Washington DC, 2010; Vol. *8*. (b) World Health Organisation report. *WHO Air Quality Guidelines for Particulate Matter, Ozone, Nitrogen Dioxide and Sulfur Dioxide*, 2005. (c) Huang, H. *Int. J. Environ. Stud.* **1992**, *41*, 267−275.

(4) Lee, J.-Y.; Keener, T. C.; Yang, Y. J. *J. Air Waste Manage. Assoc.* **2009**, *59*, 725−732.

(5) (a) Deng, H.; Yi, H.; Tang, X.; Yu, Q.; Ning, P.; Yang, L. *Chem. Eng. J.* **2012**, *188*, 77−85. (b) Matito-Martos, I.; Martin-Calvo, A.; Gutiérrez-Sevillano, J. J.; Haranczyk, M.; Doblare, M.; Parra, J. B.; Ania, C. O.; Calero, S. *Phys. Chem. Chem. Phys.* **2014**, *16*, 19884−19893.

(6) Zhang, Z.; Wu, L.; Dong, J.; Li, B.-G.; Zhu, S. *Ind. Eng. Chem. Res.* **2009**, *48*, 2142−2148.

(7) Xia, L.; Cui, Q.; Suo, X.; Li, Y.; Cui, X.; Yang, Q.; Xu, J.; Yang, Y.; Xing, H. *Adv. Funct. Mater.* **2018**, *28*, 1704292.

(8) Yi, H.; Wang, Z.; Liu, H.; Tang, X.; Ma, D.; Zhao, S.; Zhang, B.; Gao, F.; Zuo, Y. *J. Chem. Eng. Data* **2014**, *59*, 1556−1563.

(9) Yaghi, O. M.; O'Keeffe, M.; Ockwig, N. W.; Chae, H. K.; Eddaoudi, M.; Kim, J. *Nature* **2003**, *423*, 705−714.

(10) Zhou, H.-C.; Long, J. R.; Yaghi, O. M. *Chem. Rev.* **2012**, *112*, 673−674.

(11) (a) Li, J.-R.; Sculley, J.; Zhou, H.-C. *Chem. Rev.* **2012**, *112*, 869−932. (b) Li, H.; Wang, K.; Sun, Y.; Lollar, C. T.; Li, J.; Zhou, H.-C. *Mater. Today* **2018**, *21*, 108−121. (c) Lin, R.-B.; Xiang, S.; Xing, H.; Zhou, W.; Chen, B. *Coord. Chem. Rev.* **2017**, DOI: 10.1016/j.ccr.2017.09.027.

(12) Cavka, J. H.; Jakobsen, S.; Olsbye, U.; Guillou, N.; Lamberti, C.; Bordiga, S.; Lillerud, K. P. *J. Am. Chem. Soc.* **2008**, *130*, 13850−13851.

(13) Planas, N.; Mondloch, J. E.; Tussupbayev, S.; Borycz, J.; Gagliardi, L.; Hupp, J. T.; Farha, O. K.; Cramer, C. J. *J. Phys. Chem. Lett.* **2014**, *5*, 3716−3723.

(14) Wang, B.; Yang, Q.; Guo, C.; Sun, Y.; Xie, L.-H.; Li, J.-R. *ACS Appl. Mater. Interfaces* **2017**, *9*, 10286−10295.

(15) Wang, T. C.; Vermeulen, N. A.; Kim, I. S.; Martinson, A. B. F.; Stoddart, J. F.; Hupp, J. T.; Farha, O. K. *Nat. Protoc.* **2016**, *11*, 149−162.

(16) Piscopo, C. G.; Polyzoidis, A.; Schwarzer, M.; Loebbecke, S. *Microporous Mesoporous Mater.* **2015**, *208*, 30−35.

(17) Yang, S.; Liu, L.; Sun, J.; Thomas, K. M.; Davies, A. J.; George, M. W.; Blake, A. J.; Hill, A. H.; Fitch, A. N.; Tang, C. C.; Schröder, M. *J. Am. Chem. Soc.* **2013**, *135*, 4954−4957.

(18) Tan, K.; Canepa, P.; Gong, Q.; Liu, J.; Johnson, D. H.; Dyevoich, A.; Thallapally, P. K.; Thonhauser, T.; Li, J.; Chabal, Y. *Chem. Mater.* **2013**, *25*, 4653−4662.

(19) Trickett, C. A.; Helal, A.; Al-Maythalony, B. A.; Yamani, Z. H.; Cordova, K. E.; Yaghi, O. M. *Nat. Rev. Mater.* **2017**, *2*, 17045.

(20) (a) Cui, X.; Yang, Q.; Yang, L.; Krishna, R.; Zhang, Z.; Bao, Z.; Wu, H.; Ren, Q.; Zhou, W.; Chen, B.; Xing, H. *Adv. Mater.* **2017**, *29*, 1606929. (b) Savage, M.; Cheng, Y.; Easun, T. L.; Eyley, J. E.; Argent, S. P.; Warren, M. R.; Lewis, W.; Murray, C.; Tang, C. C.; Frogley, M. D.; Cinque, G.; Sun, J.; Rudić, S.; Murden, R. T.; Benham, M. J.; Fitch, A. N.; Blake, A. J.; Ramirez-Cuesta, A. J.; Yang, S.; Schröder, M. *Adv. Mater.* **2016**, *28*, 8705−8711.

(21) (a) Wu, H.; Shen Chua, Y. S.; Krungleviciute, V.; Tyagi, M.; Chen, P.; Yildirim, T.; Zhou, W. *J. Am. Chem. Soc.* **2013**, *135*, 10525−10532. (b) Chevreau, H.; Liang, W.; Kearley, G. J.; Duyker, S. G.; D'Alessandro, D. M.; Peterson, V. K. *J. Phys. Chem. C* **2015**, *119*, 6980−6987.

(22) Post, B.; Schwartz, R. S.; Fankuchen, I. *Acta Crystallogr.* **1952**, *5*, 372−374.

DOI: 10.1021/jacs.8b08433
J. Am. Chem. Soc. 2018, 140, 15564−15567